Geophysical Research Letters

RESEARCH LETTER
10.1029/2021GL097538

Special Section:
Southern Ocean and Climate: Biogeochemical and Physical Fluxes and Processes

Southern Ocean Phytoplankton Stimulated by Wildfire Emissions and Sustained by Iron Recycling

Jakob Weis[1,2], Christina Schallenberg[1,3], Zanna Chase[1], Andrew R. Bowie[1,3], Bozena Wojtasiewicz[3,4], Morgane M. G. Perron[1], Marc D. Mallet[1,3], and Peter G. Strutton[1,2]

[1]Institute for Marine and Antarctic Studies, University of Tasmania, Hobart, TAS, Australia, [2]Australian Research Council Centre of Excellence for Climate Extremes, University of Tasmania, Hobart, TAS, Australia, [3]Australian Antarctic Program Partnership, University of Tasmania, Hobart, TAS, Australia, [4]CSIRO Oceans & Atmosphere, Hobart, TAS, Australia

Abstract Large ash plumes emitted by the 2019–2020 Australian wildfires were associated with a widespread phytoplankton bloom in the iron-limited Pacific sector of the Southern Ocean. In this study, we used satellite observations and aerosol reanalysis products to study the regional phytoplankton community response to wildfire emissions. The bloom was stimulated by pyrogenic iron fertilization and coincided with elevated cellular pigment concentrations, increased photochemical efficiency, and apparent community structural shifts. Physiological anomalies were consistent with previously observed phytoplankton responses to iron stress relief and persisted for up to 9 months. Supported by a regional iron budget, we conclude that the bloom was sustained by iron recycling and episodic inputs of pyrogenic and dust-borne mineral iron. The continuous regeneration of iron was likely facilitated by the bloom's large size, mitigating edge dilution effects, as well as enhanced bioavailability of pyrogenic and mineral iron due to atmospheric and chemical processing during long-range transport.

Plain Language Summary Phytoplankton are the "plant" plankton at the base of the ocean food chain. Phytoplankton growth in the Southern Ocean is limited by the availability of iron. Deserts and wildfires are two important sources of iron-bearing particles that can be transported over long distances and deposited on the ocean surface, causing increased phytoplankton growth and species changes. In this study we used observations from satellites to study the physiological response of a large phytoplankton bloom stimulated by emissions from the 2019–2020 Australian wildfires. We found the cells became richer in pigments, and more efficient in their photosynthesis. The changes are directly attributable to wildfire emissions and correspond with previously observed phytoplankton responses to iron fertilization experiments and natural fertilization by dust, volcanic ash, and upwelled iron from the deep ocean. The phytoplankton response lasted almost half a year after wildfire particles stimulated the bloom. We attribute the prolonged response in part to iron recycling, re-supplying dissolved iron inside the bloom, and to additional deposition of wildfire emissions and dust.

Key Points:

- 2019–2020 Australian wildfire emissions stimulated phytoplankton community responses consistent with iron fertilization
- Physiological anomalies lasted 9 months and were sustained by iron recycling and atmospheric iron supply by dust and wildfire emissions
- Atmospheric processing of wildfire emissions likely increased the solubility of pyrogenic iron, amplifying its effect on the phytoplankton

Supporting Information:

Supporting Information may be found in the online version of this article.

Correspondence to:

J. Weis,
jakob.weis@utas.edu.au

Citation:

Weis, J., Schallenberg, C., Chase, Z., Bowie, A. R., Wojtasiewicz, B., Perron, M. M. G., et al. (2022). Southern Ocean phytoplankton stimulated by wildfire emissions and sustained by iron recycling. *Geophysical Research Letters*, *49*, e2021GL097538. https://doi.org/10.1029/2021GL097538

Received 21 DEC 2021
Accepted 20 MAY 2022

Author Contributions:

Conceptualization: Jakob Weis, Christina Schallenberg, Zanna Chase, Andrew R. Bowie, Bozena Wojtasiewicz, Morgane M. G. Perron, Marc D. Mallet, Peter G. Strutton

1. Introduction

Primary productivity in the Southern Ocean is seasonally limited by iron and light (Boyd, 2002; Martin et al., 1990; Mitchell et al., 1991; Ryan-Keogh et al., 2018). Supply of bioavailable iron to surface waters is largely dependent on upwelling of iron-rich subsurface waters (Schallenberg et al., 2018; Tagliabue et al., 2014) and deposition of iron-bearing aerosols from dust storms (Jickells et al., 2005; Mahowald et al., 2005), wildfires (Mallet et al., 2017; Perron et al., 2020, 2022), and volcanic eruptions (Olgun et al., 2011; Perron et al., 2021). Iron recycling is a secondary yet substantial source of bioavailable iron and allows phytoplankton to maintain standing stocks for up to several weeks without new external supply of iron (Bowie et al., 2001; Boyd et al., 2015; Laglera et al., 2017). The role of iron retention through recycling is particularly important in large-scale fertilization events, due to the reduced impact of dilution with ambient waters at the bloom edges (Abraham et al., 2000; Brzezinski et al., 2005).

Distinct changes in ocean surface optical properties have been attributed to the phytoplankton response to ocean iron fertilization (OIF) experiments (Westberry et al., 2013), iron addition from subsurface waters (Schallenberg et al., 2018; Westberry et al., 2013), and fertilization by dust (Gabric et al., 2016) and volcanic ash (Achterberg et al., 2013; Hamme et al., 2010; Westberry et al., 2019). The ocean fertilization potential of large-scale wildfires has been previously hypothesized (Abram et al., 2003; Hamilton et al., 2022; Ito et al., 2021) based on

Data curation: Jakob Weis
Formal analysis: Jakob Weis
Funding acquisition: Zanna Chase, Andrew R. Bowie, Peter G. Strutton
Investigation: Jakob Weis
Methodology: Jakob Weis
Project Administration: Christina Schallenberg, Zanna Chase, Andrew R. Bowie, Peter G. Strutton
Supervision: Christina Schallenberg, Zanna Chase, Andrew R. Bowie, Peter G. Strutton
Validation: Jakob Weis
Visualization: Jakob Weis
Writing – original draft: Jakob Weis
Writing – review & editing: Jakob Weis, Christina Schallenberg, Zanna Chase, Andrew R. Bowie, Bozena Wojtasiewicz, Morgane M. G. Perron, Marc D. Mallet, Peter G. Strutton

the elevated bioavailable iron content of wildfire emissions (Perron et al., 2020; Winton et al., 2016) and their propensity for long-range transport (Zheng & Sohrin, 2019), as well as paleo-reconstructions of wildfire-supported phytoplankton productivity (Liu et al., 2022). Direct observations of the phytoplankton response to wildfire emissions, however, are scarce and predominantly derived from chlorophyll, carbon biomass or local changes in phytoplankton community composition (Kramer et al., 2020; Tang et al., 2021; W. Wang et al., 2021; Y. Wang et al., 2022), leaving the physiological response uninvestigated.

Between September 2019 and March 2020, the Australian wildfires injected large amounts of iron-bearing aerosols into the atmosphere, which were transported across the southern hemisphere, reaching remote parts of the iron-limited South Pacific within days, where they stimulated widespread chlorophyll anomalies (Tang et al., 2021; Y. Wang et al., 2022). In this study, we investigated the phytoplankton community response and the regional iron cycle in greater detail, to address the following questions: How did the regional phytoplankton community respond to the fertilization by wildfire emissions? How does this response compare to iron fertilization from other sources? And to what extent have additional iron sources contributed to the bloom's longevity by maintaining elevated bioavailable iron concentrations at the ocean surface? Answers to these questions will provide valuable insights into the ecosystem response to wildfire-induced ocean fertilization and the long-lasting impact of widespread iron supply on phytoplankton and on the oceanic iron cycle.

2. Methods

Anomalies of aerosol deposition and the phytoplankton response were quantified by comparing 2019–2020 satellite and reanalysis data against 17-year (2002–2018) climatological records that preceded the study period. Time series were averaged over the bloom region, 37°S–50°S and 150°W–90°W (Figure 1). The bloom was defined according to Behrenfeld and Boss (2018). Relative anomalies were determined by subtracting climatologies from 2019–2020 observations and normalizing this difference to the climatology.

2.1. Aerosol Deposition Flux

Daily, 0.5 × 0.65° resolved aerosol data were obtained from the Modern-Era Retrospective Analysis for Research and Applications, Version 2 (MERRA-2; Gelaro et al., 2017). Black carbon (BC) and dust deposition fluxes were used as proxies for wildfire emissions and mineral dust, respectively. The total aerosol deposition flux was calculated as the sum of wet and dry deposition of BC (hydrophilic and hydrophobic) and dust (0.1–10 μm particle radius). Pyrogenic and mineral iron (collectively referred to as aerosol-iron) deposition fluxes were derived from BC and dust deposition, respectively, using an Fe:BC ratio of 0.15, a literature-based iron content in mineral dust (3.5 weight-%; Mahowald et al., 2005) and aerosol-specific fractional iron solubilities (20%–80% and 5%–30% of total pyrogenic and mineral iron, respectively; Ito et al., 2019; Perron et al., 2020; Winton et al., 2016).

2.2. Bio-Optical Parameters

Weekly (8-day), 0.042° resolved bio-optical observations, made by the Moderate Resolution Imaging Spectroradiometer aboard the NASA satellite Aqua (MODIS-Aqua), were used to analyze the phytoplankton response throughout the bloom period. A 3-week moving mean was applied to reduce the impact of cloud coverage. Phytoplankton abundance was derived from surface concentrations of chlorophyll (chl) and phytoplankton carbon biomass (C_{phyto}). C_{phyto} was derived from the particulate backscattering coefficient, b_{bp}, at 443 nm: $C_{phyto} = b_{bp} \times 13000 - 4.55$ (Behrenfeld et al., 2005).

The physiological response to changing environmental conditions was derived from two ratios. Chl per unit carbon (chl:C_{phyto}) reflects community-wide changes in cellular pigmentation, inferred from differing rates of change of surface pigment and biomass concentration. An increase in chl:C_{phyto} is commonly attributed to nutrient stress relief (Gall et al., 2001; Halsey & Jones, 2015; Hoffmann et al., 2006) and reduced light availability (Falkowski & LaRoche, 1991; Geider et al., 1996). Phytoplankton fluorescence per unit chl (nFLH:chl), corrected for non-photochemical quenching based on sea surface temperature (Browning et al., 2014), was used to derive community-wide changes in the fluorescence quantum yield (emitted vs. absorbed light; Behrenfeld et al., 2009).

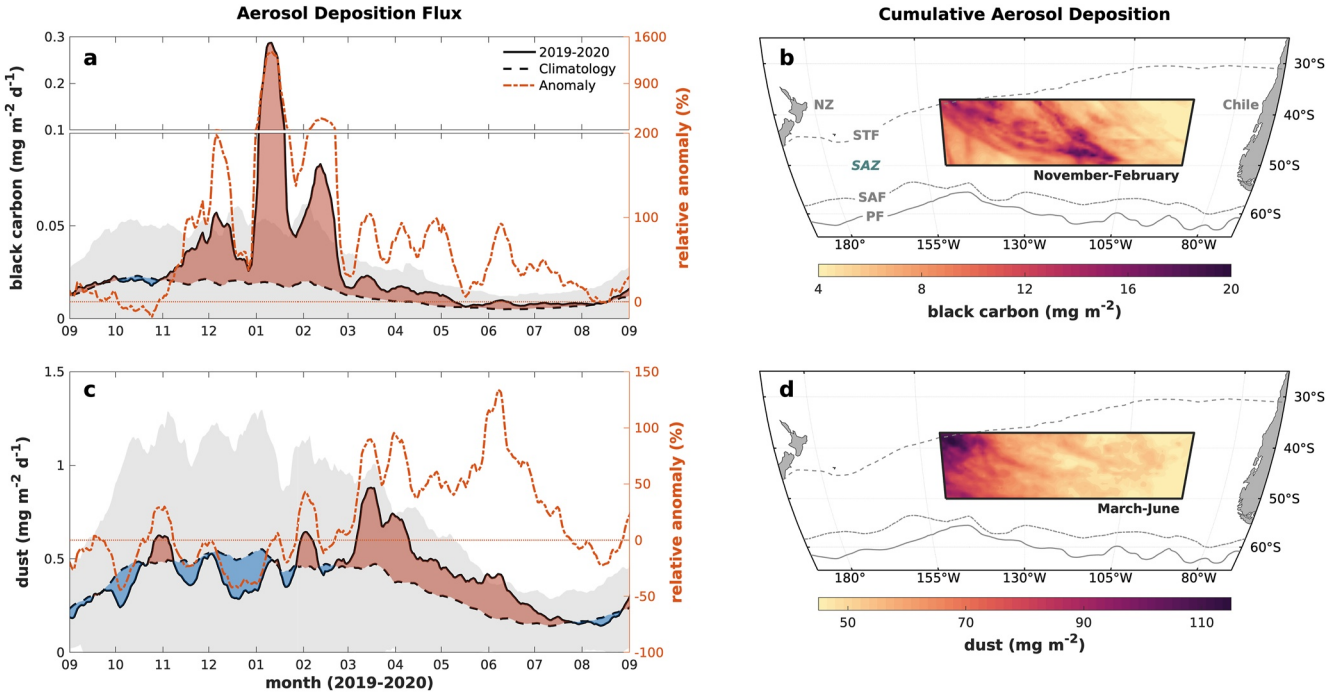

Figure 1. Black carbon (BC) and dust deposition over the Pacific sector of the Southern Ocean during the 2019–2020 austral summer. (a and c), September 2019–2020 BC and dust deposition fluxes averaged over the bloom region (solid lines). Climatological fluxes and standard deviations are shown as dashed lines and gray shades. Red and blue shaded areas indicate positive and negative anomalies. Relative 2019–2020 anomalies are plotted on the secondary *Y*-axis (red dash-dotted lines). (b and d), Cumulative BC and dust deposition on the bloom region integrated over their respective peak deposition periods. Gray lines indicate, from north to south, the locations of the subtropical front, the subantarctic zone, the subantarctic front, and the polar front (Orsi et al., 1995).

A decrease in nFLH:chl reflects more favorable nutrient conditions (Behrenfeld & Milligan, 2013). We assume a well-mixed surface ocean in which the satellite-derived phytoplankton response at the surface reflects the response in the mixed layer or euphotic zone (the shallower of the two).

Relative phytoplankton community changes were assessed based on the backscatter slope (S_{bp}). S_{bp} is the spectral power-law slope of b_{bp} and its relation to community structural shifts stems from the assumption that the b_{bp} signal is related to particle shape and size and therefore species-dependent (Bohren, 1983; Vaillancourt et al., 2004; Whitmire et al., 2010).

2.3. Mixed Layer Irradiance

The effect of changing light conditions on chl:C_{phyto} was qualitatively assessed based on the median mixed layer irradiance (I_{ML}). I_{ML} is a measure of light availability at the center of the mixed layer and a function of the photosynthetically available radiation (PAR), the diffuse attenuation of downwelling irradiance (Kd) and the mixed layer depth (MLD): $I_{ML} = \text{PAR} \times e^{-0.5 \times \text{MLD} \times \text{Kd}}$ (Behrenfeld et al., 2016). PAR and Kd are MODIS-Aqua products and the regional MLD was derived from in situ Argo float measurements. We used an Argo mixed layer climatology compiled by Holte et al. (2017). We refrained from correcting chl:C_{phyto} using a photo-acclimation model due to the poor performance of these models in the Southern Ocean (Behrenfeld et al., 2016).

2.4. Dissolved Iron Budget

Satellite net primary production, NPP (based on the Eppley-VGPM algorithm; Behrenfeld & Falkowski, 1997), was used to determine the mass balance between the anomalous biological iron demand (uptake) and its anomalous supply from recycled and atmospheric sources in the study region. Iron uptake (μmol m^{-2} d^{-1}) was determined by multiplying NPP (mol carbon m^{-2} d^{-1}) by an Fe:C uptake ratio (6–20 μmol mol^{-1}; Twining et al., 2004). The loss

of iron exported to depth was derived from export efficiencies, defined as the fraction of biomass exported below 100 m. Export efficiencies (e-ratio) were calculated from NPP using a log-linear relationship to Eppley-VGPM NPP specific to the subantarctic zone (SAZ): e-ratio = $-0.69 \times \log_{10}(\text{NPP}) + 2.03$ (Fan et al., 2020). Recycling fluxes were estimated from recycling rates (10%–70% of un-exported iron; Bowie et al., 2009). Solving the mass balance for the atmospheric supply term (i.e., the difference between uptake and recycled supply) allowed us to model atmospheric dFe anomalies required to balance the bloom's increased dFe demand (see Text S1 in Supporting Information S1 for a detailed model description).

3. Results and Discussion

3.1. Elevated Black Carbon and Dust Deposition on the South Pacific

Throughout the 2019–2020 austral summer and autumn, the Pacific sector of the Southern Ocean was exposed to sustained and anomalously high deposition of BC and mineral dust (Figure 1). BC and dust deposition time series averaged over the study region reveal two distinct aerosol deposition periods. From November to February, 62,000 tonnes of BC were deposited on the eastern South Pacific in three events (Figures 1a and 1b). The majority of BC was deposited in January, when fluxes temporarily exceeded the climatology by more than 1,300%. In March, as the wildfires abated, BC deposition fluxes decreased but remained up to twice as high as the climatology until July. Concurrently, an increase in dust deposition was observed over the bloom region, with fluxes exceeding the climatology by 50%–150% before returning to climatological conditions in July (Figures 1c and 1d).

Analysis of aerosols collected in southern Tasmania, Australia, in December and January, showed that the wildfire emissions were associated with elevated concentrations of soluble iron (Perron et al., 2022). Iron emitted during the wildfires was predominantly contained in soil particles entrained in the fire plumes by pyro-convective winds (Bodí et al., 2014; Wagner et al., 2018) and processed by the heat and acidity of the fire fumes (Baker et al., 2021; Balasubramanian et al., 1999; Perron et al., 2022). Pyro-convective updraft of soil may account for more than 60% of the pyrogenic iron emitted during wildfires (Hamilton et al., 2022).

Dust emissions are known to increase in the aftermath of wildfires due to increased exposure of bare soil (Dukes et al., 2018; Whicker et al., 2006). The MERRA-2 aerosol reanalysis calculates dust emissions based on surface winds over pre-defined dust source regions, which mainly encompass the Australian deserts (Randles et al., 2017). It therefore does not account for enhanced dust emission from wildfire-impacted regions due to updraft or devegetation.

Strongly light-absorbing aerosols interfere with ocean color measurements, which can result in an overestimation of satellite-derived chl (Frouin et al., 2019; Schollaert et al., 2003). These biases are partly corrected for during NASA's post-processing (Mobley et al., 2016). Due to the localized and episodic nature of the ash plumes, any remaining artifacts occur at significantly smaller spatial and temporal scales than the basin-scale, 3-weekly averaged time series discussed here and are therefore not expected to bias our observations significantly.

3.2. Pyrogenic Iron Stimulated Phytoplankton Biomass and Pigment Production

The deposition of wildfire aerosols was immediately followed by positive chl and C_{phyto} anomalies. From early November to late January, concurrent with the first two fire plumes, surface chl doubled, exceeding climatological concentrations by up to 177% (0.26 mg m^{-3}, Figure 2a). Hereafter, chl anomalies declined gradually, but remained 20% higher than the climatology until early July. C_{phyto} anomalies were smaller than chl anomalies, but correspondingly increased with the arrival of the first fire plume in November and December (36% peak anomaly), and returned to climatological conditions by April (Figure 2b). These anomalies agree with in situ chl and b_{bp} anomalies observed by biogeochemical Argo floats profiling the eastern bloom region (Figure S5 and Text S2 in Supporting Information S1; Tang et al., 2021) and are consistent with satellite-detected biological responses to purposeful and natural OIF (Westberry et al., 2013). The anomalies also exceeded anomalies observed after volcanic ash fertilization in the North Pacific (Westberry et al., 2019), likely due to higher soluble iron concentrations in wildfire emissions compared to volcanic ash (Hamilton et al., 2022; Ito et al., 2019; Perron et al., 2021) as well as stronger iron deficiency in the South Pacific compared to the North Pacific (Abadie et al., 2017; Zheng & Sohrin, 2019).

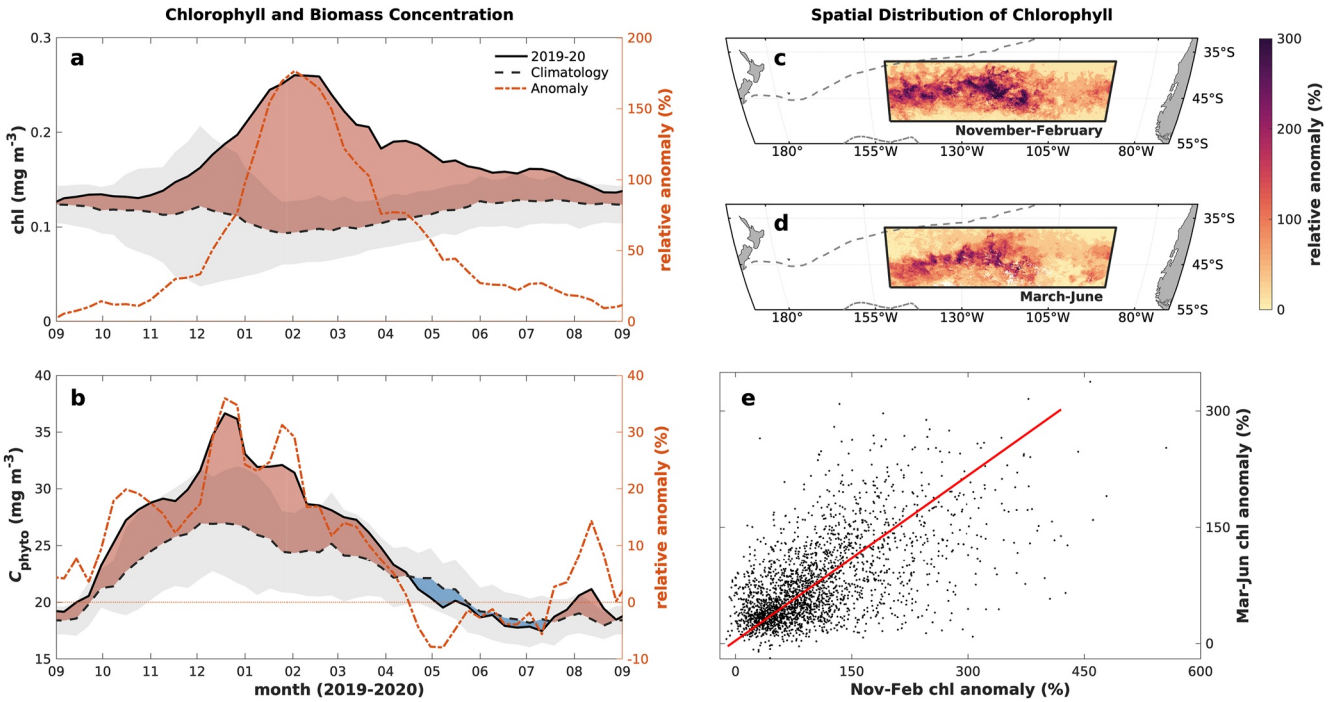

Figure 2. Chlorophyll and biomass accumulation in the bloom region. (a and b), 2019–2020 observations, climatologies and relative anomalies of surface chlorophyll (chl) and phytoplankton carbon (C_{phyto}) averaged over the bloom region (lines and shaded areas correspond with Figure 1). (c and d), Spatial distribution of average chl anomalies from November–February and from March–June. Ocean fronts are denoted in Figure 1. (e), Pixel-by-pixel correlation between chl anomalies shown in panels c and d (p-value < 0.01, $R^2 = 0.36$).

3.3. Increased Cellular Pigmentation Induced by Iron Stress Relief

Differences in timing and magnitude of the chl and C_{phyto} anomalies reveal distinct physiological responses of the phytoplankton community to pyrogenic iron input. C_{phyto} anomalies peaked 6 weeks earlier, returned to climatological levels 3 months earlier, and were consistently smaller than chl anomalies. Reflecting these differences, chl:C_{phyto} reached peak anomalies in mid-January (132%, Figure 3a), coinciding with anomalously high pyrogenic aerosols and consistent with elevated in situ chl:b_{bp} measured by BGC-Argo floats (Figure S5 in Supporting Information S1; Tang et al., 2021).

The observed increase in cellular pigmentation was likely the result of two separate phytoplankton acclimation responses. The initial increase in cellular pigment production was induced by the relief of iron stress, allowing for increased growth rates of the invigorated phytoplankton community (Gall et al., 2001; Halsey & Jones, 2015; Hoffmann et al., 2006). As a result, light attenuation (Kd) by organic matter and light-absorbing pigments at the surface led to depressed mixed layer light levels (I_{ML}; Figure 3c), causing an additional increase in cellular pigmentation as phytoplankton adapted to the reduced light availability (photo-acclimation; Falkowski & LaRoche, 1991; Geider et al., 1996). MLDs and PAR (additional factors controlling I_{ML}) were at near-climatological levels throughout the study period (Figure S1 in Supporting Information S1), suggesting that the photo-acclimation response was largely caused by the bloom itself. Interestingly, the peak in chl:C_{phyto} in February occurred close in time to the seasonal maximum in light when cellular pigmentation is expected to be at its lowest, further highlighting the anomalous nature of the physiological response. The strong increase in chl due to the combined effects of phytoplankton growth and increased cellular pigmentation may have eventually led to self-shading and stagnation of growth (Sakshaug et al., 1991; Twelves et al., 2021), causing the observed time difference between the C_{phyto} and chl peak (Figure 2).

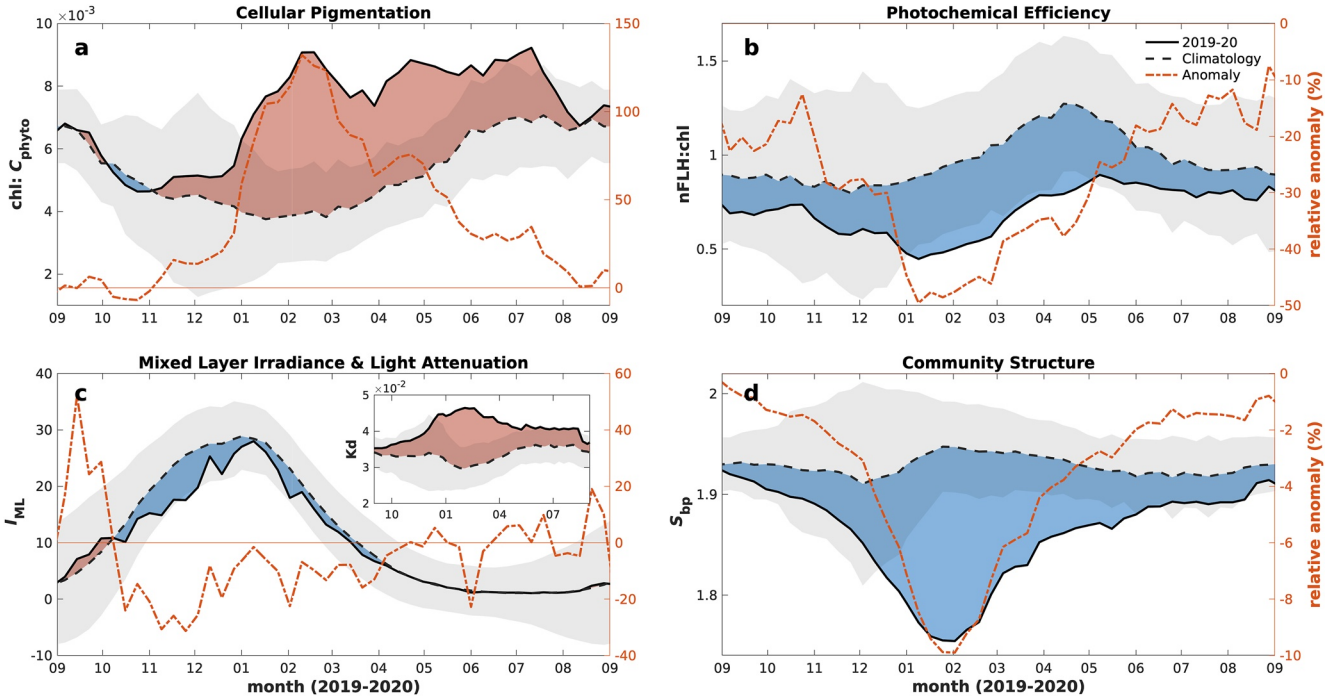

Figure 3. Anomalous phytoplankton physiology, community structure and mixed layer light conditions in the bloom region. (a, b, and d), 2019–2020 observations, climatologies and relative anomalies of the chlorophyll to carbon ratio, chl:C_{phyto}, the NPQ-corrected fluorescence to chlorophyll ratio, nFLH:chl (mW m^{-3} cm^{-2} μm^{-1} sr^{-1} (mg chl)$^{-1}$) and the spectral backscatter slope, S_{bp}. (c), Median mixed layer irradiance, I_{ML} (Ein m^{-2} d^{-1}) and the diffuse attenuation of downwelling irradiance, Kd (m^{-1}). Lines and shaded areas correspond with previous figures. Negative nFLH:chl anomalies indicate an increase in photochemical efficiency.

3.4. Increased Photochemical Efficiency and Community Structural Shifts

Further information about the bloom physiology can be gained from phytoplankton fluorescence normalized to chl, nFLH:chl (Figure 3b), a proxy for the fluorescence quantum yield. We observed anomalously low nFLH:chl between November and January, coinciding with elevated fire emissions and other physiological anomalies. nFLH:chl is commonly used to estimate the photochemical efficiency (Westberry et al., 2013, 2019) and, like chl:C_{phyto}, it responds to changes in iron availability. Following iron stress relief, excess pigments are activated for photosynthesis, reducing phytoplankton fluorescence and lowering nFLH:chl (Behrenfeld & Milligan, 2013).

Lastly, we qualitatively assessed variations in the phytoplankton community based on S_{bp} (Figure 3d). Distinct negative S_{bp} anomalies between December and May suggest an anomalous shift of the phytoplankton community during the peak of the bloom. While we were unable to investigate the community structure in further detail, the coincidence of the S_{bp} anomalies with pyrogenic iron supply and related biological responses (all anomalies compiled in Figure S4 in Supporting Information S1) leads us to attribute the observed community shift to changes in phytoplankton species composition following iron stress relief (Armand et al., 2008; Wolff et al., 2011). Low silicic acid levels in the SAZ (Hiscock et al., 2003) likely favored weakly silicified and calcifying phytoplankton groups (prymnesiophytes, pelagophytes, dinoflagellates, *Pseudonitzschia* spp.), as documented during the Southern Ocean Iron Experiment north patch in low-iron, low-silicic acid South Pacific waters (Coale et al., 2004).

3.5. Iron Recycling, Wildfire Emissions and Dust Sustained the Bloom for 9 Months

A particularly interesting feature of the time series is the gradual decline of the biological response persisting until July, despite the sudden drop in wildfire emissions in early March. To reconcile the longevity of the bloom with the sudden reduction of pyrogenic iron, additional iron sources need to be considered. Iron supply to the ocean surface from volcanic ash (Duggen et al., 2010), sedimentary sources (Tagliabue et al., 2009), upwelling (Morrison et al., 2015) and vertical diffusion (Tagliabue et al., 2014) are of limited relevance in the central South Pacific and have therefore been discounted as additional sources. Iron supply by deep mixing can be considerable, but mainly plays a role south of the polar front and during winter months (Tagliabue et al., 2014). Furthermore,

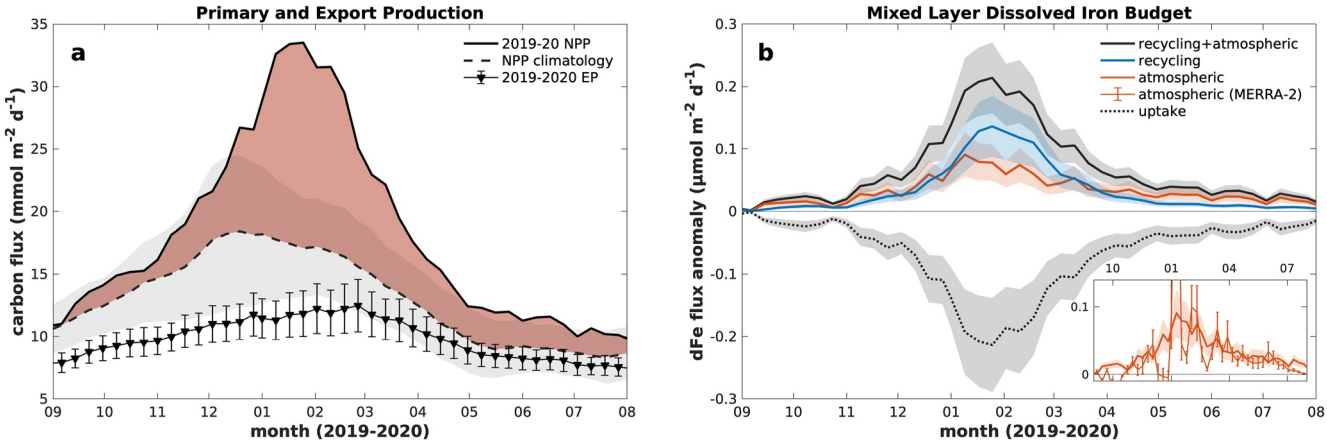

Figure 4. Primary production, export, and a mixed layer dissolved iron (dFe) budget of the bloom. (a), 2019–2020 satellite net primary production and export production. Lines and shaded areas correspond with previous figures. (b), The modeled regional mass balance between the anomalous biological dFe demand (dotted line, shown as negative fluxes) and its supply through recycling and atmospheric deposition (solid lines). Inset: Mass-balanced anomalous atmospheric dFe fluxes compared against MERRA-2-derived atmospheric dFe anomalies (dashed line). MERRA-2 fluxes are the sum of aerosol-derived mineral and pyrogenic dFe fluxes. Uncertainties introduced by variable model parameters are shown as envelopes and error bars (see Text S1.4 in Supporting Information S1).

between January and July the mixed layer was shallower than average (Figure S1c in Supporting Information S1). Thus, mixing was unlikely to have contributed significantly to the observed biological anomalies. This leaves mineral dust and iron recycling as the two remaining iron sources. Elevated dust deposition from March to July (Figure 1c) suggests that mineral iron, together with pyrogenic iron, had the potential to fuel the bloom during its later stages. Statistically significant pixel-by-pixel correlations between spatially resolved bio-optical anomalies averaged over the first and the second half of the bloom suggest that the phytoplankton response was largely stationary (Figures 2c–2e, S2, and S3 in Supporting Information S1), an expected feature if the bloom was relying on regenerated iron. Previous studies have demonstrated the importance of iron recycling after fertilization events, prolonging the phytoplankton response for days to several weeks (Barbeau et al., 2001; Bowie et al., 2001; Hutchins et al., 1993; Laglera et al., 2017; Westberry et al., 2019).

3.6. A Regional Mixed Layer Dissolved Iron Budget

To test our hypothesis that the anomalous phytoplankton response was sustained by iron recycling and aerosol-iron deposition, we developed a mixed layer dissolved iron (dFe) budget for the bloom region using a simple model (Figure 4, Text S1 in Supporting Information S1). Anomalously high NPP throughout the bloom period implies both an elevated biological demand for dFe and an increased supply of dFe by iron recycling (Figure 4a). Assuming Fe:C uptake ratios of 6–20 µmol mol^{-1} (Twining et al., 2004), the dFe consumption of the phytoplankton community would have exceeded climatological demands by up to 0.21 ± 0.08 µmol m^{-2} d^{-1} (Figure 4b). At recycling rates of 10%–70% (Bowie et al., 2009), regenerated dFe supplied a significant proportion of the increased biological demand and was likely the dominant iron source during the peak of the bloom in January and February.

Mass-balanced anomalous atmospheric dFe fluxes, calculated as the difference between the biological demand and the recycled supply, agree in magnitude with MERRA-2-derived aerosol-iron inputs (Figure 4b inset). The assumed Fe:BC ratio of 0.15, used to determine pyrogenic iron deposition, is higher than the global average (0.06; Hamilton et al., 2019), consistent with increased entrainment of iron-rich mineral dust in the smoke plumes (Kablick et al., 2020; Perron et al., 2022). Soluble pyrogenic and mineral iron fractions (20%–80% and 5%–30%, respectively) are at the upper end of literature values (Ito et al., 2019; Perron et al., 2020; Winton et al., 2016), too, which can be explained by an increase in iron solubility by atmospheric processing during long-range transport (Shi et al., 2011), particularly in the Southern Hemisphere (Ito et al., 2019). High temperatures and strong acidity of wildfire plumes are expected to have further increased the iron solubility of wildfire emissions (Baldo et al., 2022; Perron et al., 2022).

The mass-balanced atmospheric dFe fluxes assume a constant supply of iron which does not reflect the episodic nature of mineral and pyrogenic iron deposition. The strongly fluctuating MERRA-2-derived atmospheric dFe fluxes suggest alternating periods of iron excess and deficiency relative to the demand (Figure 4 inset). We hypothesize that excess dFe accumulated during deposition events because consumption was constrained by physical and chemical uptake limits (Sunda & Huntsman, 1995), macro-nutrient limitation (Sedwick et al., 2002) or light limitation (see above, 3.3). Assuming that excess dFe was retained at the surface, it could have sustained the bloom during periods of low external iron input. This assumption implies dFe residence times at the surface on the order of weeks to months. Such residence times are consistent with previously published estimates (Black et al., 2020; Hayes et al., 2015) and were likely facilitated by atmospheric processing and grazer-mediated solubility enhancement (Barbeau & Moffett, 2000; Barbeau et al., 1996) and an abundance of iron-binding ligands (Boye et al., 2001; Thuróczy et al., 2011), which are continuously being resupplied during recycling (Croot et al., 2001; Hogle et al., 2016; Sato et al., 2007), preventing iron from being scavenged to sinking particulates.

The iron budget substantiates our hypothesis that the phytoplankton bloom was sustained for nearly 9 months by iron recycling and sporadically fueled by aerosol-iron inputs from wildfire emissions and dust—a remarkable feature which has rarely been observed before on such long time scales (Westberry et al., 2019). Given the budget's robustness to a wide range of environmental parameters, it would require unrealistic environmental conditions to sustain the bloom for 9 months without recycled iron. The extensive initial supply of highly soluble pyrogenic iron and the widespread nature of the bloom were essential prerequisites for the prolonged recycling of iron, reducing the influence of dilution at the bloom edges (Abraham et al., 2000; Brzezinski et al., 2005), thus allowing for iron to be retained in the fertilized patch.

4. Conclusion

This case study reveals the far-reaching impact of the 2019–2020 Australian wildfires on phytoplankton in the iron-limited Pacific sector of the Southern Ocean. We analyzed the phytoplankton biomass, physiology, and community structure following iron enrichment by wildfire emissions and dust, in the context of nearly two decades of bio-optical satellite observations and reanalysis data. The results of the bio-optical analysis provide valuable insights into the ecosystem response to wildfire-driven OIF. Physiological anomalies (increase in cellular pigmentation and photochemical efficiency, community structural shift), previously only observed in relation to purposeful OIF, sub-surface iron supply, dust storms and volcanic eruptions, are conclusively attributable to particle emissions by wildfires and lasted nearly 9 months.

Another striking feature of the bloom was its longevity. Following its initiation by pyrogenic iron between November 2019 and February 2020, recycling played an important role in retaining bio-available iron in the fertilized regions and maintaining the bloom as the wildfires abated and pyrogenic iron supply was reduced. Dissolved iron was continuously regenerated inside the bloom for nearly 9 months, until July 2020, and sporadically re-supplied by episodic deposition of continuing pyrogenic inputs and mineral iron from dust. We attribute the immediate and widespread biological response to highly soluble iron from fire emissions, following atmospheric transport and processing by the strong heat and acidity of the wildfire plumes. The month-long retention of iron in the bloom region was facilitated by reduced edge dilution due to the large extent of the bloom.

Data Availability Statement

All data products used in this study are freely available. Aerosol reanalysis products were obtained from the NASA Goddard Earth Sciences Data and Information Service Center (GES DISC, https://goldsmr4.gesdisc.eosdis.nasa.gov/data/MERRA2/M2T1NXADG.5.12.4/). Ocean color data products (chlor_a, bbp_443_giop, nflh, bbp_s_giop, par, Kd_490, sst, ipar) were obtained from the NASA Ocean Biology Distributed Active Archive Center (OB.DAAC, https://oceandata.sci.gsfc.nasa.gov/MODIS-Aqua/Mapped/8-Day/4km/). Net primary productivity maps were obtained from the Oregon State University Ocean Productivity website (http://orca.science.oregonstate.edu/1080.by.2160.8day.hdf.eppley.m.chl.m.sst.php). Core-Argo data, used for MLD calculations, were obtained directly from the IFREMER Argo database (https://data-argo.ifremer.fr/geo/pacific_ocean/). BGC-Argo data, used in the supporting analysis of the in situ bloom response, were obtained from the US Global Ocean Data Assimilation Experiment Argo Global Data Assembly Center (USGODAE Argo GDAC, https://usgodae.org/ftp/outgoing/argo/dac) using the BGC-Argo-Mat toolbox (Frenzel et al., 2021). These data were collected and made

freely available by the International Argo Program and the national programs that contribute to it (https://argo.ucsd.edu, https://www.ocean-ops.org). The Argo Program is part of the Global Ocean Observing System.

Acknowledgments
This research was supported by the Australian Government through the Australian Research Council Discovery Grant (DP190103504) and through the Australian Antarctic Program Partnership as part of the Antarctic Science Collaboration Initiative (ASCI000002). J. Weis and P. G. Strutton are also supported by the Australian Research Council Centre of Excellence for Climate Extremes (CLEX: CE170100023). We would specifically like to acknowledge the Southern Ocean Carbon and Climate Observations and Modeling Project funded by the National Science Foundation, Division of Polar Programs (NSF PLR-1425989 and OPP-1936222), supplemented by NASA. We thank Abigail Smith and Matthew Corkill for their helpful insights on Fe-binding ligands. Open access publishing facilitated by University of Tasmania, as part of the Wiley - University of Tasmania agreement via the Council of Australian University Librarians.

References

Abadie, C., Lacan, F., Radic, A., Pradoux, C., & Poitrasson, F. (2017). Iron isotopes reveal distinct dissolved iron sources and pathways in the intermediate versus deep Southern Ocean. *Proceedings of the National Academy of Sciences of the United States of America*, *114*(5), 858–863. https://doi.org/10.1073/pnas.1603107114

Abraham, E. R., Law, C. S., Boyd, P. W., Lavender, S. J., Maldonado, M. T., & Bowie, A. R. (2000). Importance of stirring in the development of an iron-fertilized phytoplankton bloom. *Nature*, *407*(6805), 727–730. https://doi.org/10.1038/35037555

Abram, N. J., Gagan, M. K., McCulloch, M. T., Chappell, J., & Hantoro, W. S. (2003). Coral reef death during the 1997 Indian Ocean Dipole linked to Indonesian wildfires. *Science*, *301*(5635), 952–955. https://doi.org/10.1126/science.1083841

Achterberg, E. P., Moore, C. M., Henson, S. A., Steigenberger, S., Stohl, A., Eckhardt, S., et al. (2013). Natural iron fertilization by the Eyjafjallajökull volcanic eruption. *Geophysical Research Letters*, *40*(5), 921–926. https://doi.org/10.1002/grl.50221

Armand, L. K., Cornet-Barthaux, V., Mosseri, J., & Quéguiner, B. (2008). Late summer diatom biomass and community structure on and around the naturally iron-fertilised Kerguelen Plateau in the Southern Ocean. *Deep-Sea Research Part II Topical Studies in Oceanography*, *55*(5–7), 653–676. https://doi.org/10.1016/j.dsr2.2007.12.031

Baker, A. R., Kanakidou, M., Nenes, A., Myriokefalitakis, S., Croot, P. L., Duce, R. A., et al. (2021). Changing atmospheric acidity as a modulator of nutrient deposition and ocean biogeochemistry. *Science Advances*, *7*(28), eabd8800. https://doi.org/10.1126/sciadv.abd8800

Balasubramanian, R., Victor, T., & Begum, R. (1999). Impact of biomass burning on rainwater acidity and composition in Singapore. *Journal of Geophysical Research*, *104*(D21), 26881–26890. https://doi.org/10.1029/1999JD900247

Baldo, C., Ito, A., Krom, M. D., Li, W., Jones, T., Drake, N., et al. (2022). Iron from coal combustion particles dissolves much faster than mineral dust under simulated atmospheric acidic conditions. *Atmospheric Chemistry and Physics*, *22*(9), 6045–6066. https://doi.org/10.5194/acp-22-6045-2022

Barbeau, K., Kujawinski, E. B., & Moffett, J. W. (2001). Remineralization and recycling of iron, thorium and organic carbon by heterotrophic marine protists in culture. *Aquatic Microbial Ecology*, *24*(1), 69–81. https://doi.org/10.3354/ame024069

Barbeau, K., & Moffett, J. W. (2000). Laboratory and field studies of colloidal iron oxide dissolution as mediated by phagotrophy and photolysis. *Limnology & Oceanography*, *45*(4), 827–835. https://doi.org/10.4319/lo.2000.45.4.0827

Barbeau, K., Moffett, J. W., Caron, D. A., Croot, P. L., & Erdner, D. L. (1996). Role of protozoan grazing in relieving iron limitation of phytoplankton. *Nature*, *380*(6569), 61–64. https://doi.org/10.1038/380061a0

Behrenfeld, M. J., Boss, E., Siegel, D. A., & Shea, D. M. (2005). Carbon-based ocean productivity and phytoplankton physiology from space. *Global Biogeochemical Cycles*, *19*(1), GB1006. https://doi.org/10.1029/2004GB002299

Behrenfeld, M. J., & Boss, E. S. (2018). Student's tutorial on bloom hypotheses in the context of phytoplankton annual cycles. *Global change biology*, *24*(1), 55–77. https://doi.org/10.1111/gcb.13858

Behrenfeld, M. J., & Falkowski, P. G. (1997). Photosynthetic rates derived from satellite-based chlorophyll concentration. *Limnology & Oceanography*, *42*(1), 1–20. https://doi.org/10.4319/lo.1997.42.1.0001

Behrenfeld, M. J., & Milligan, A. J. (2013). Photophysiological expressions of iron stress in phytoplankton. *Annual Review of Marine Science*, *5*(1), 217–246. https://doi.org/10.1146/annurev-marine-121211-172356

Behrenfeld, M. J., O'Malley, R. T., Boss, E. S., Westberry, T. K., Graff, J. R., Halsey, K. H., et al. (2016). Revaluating ocean warming impacts on global phytoplankton. *Nature Climate Change*, *6*(3), 323–330. https://doi.org/10.1038/nclimate2838

Behrenfeld, M. J., Westberry, T. K., Boss, E. S., O'Malley, R. T., Siegel, D. A., Wiggert, J. D., et al. (2009). Satellite-detected fluorescence reveals global physiology of ocean phytoplankton. *Biogeosciences*, *6*(5), 779–794. https://doi.org/10.5194/bg-6-779-2009

Black, E. E., Kienast, S. S., Lemaitre, N., Lam, P. J., Anderson, R. F., Planquette, H., et al. (2020). Ironing out Fe residence time in the dynamic upper ocean. *Global Biogeochemical Cycles*, *34*(9), e2020GB006592. https://doi.org/10.1029/2020GB006592

Bodí, M. B., Martin, D. A., Balfour, V. N., Santín, C., Doerr, S. H., Pereira, P., & Mataix-Solera, J. (2014). *Wildland Fire Ash: Production, Composition and Eco-Hydro-Geomorphic Effects* (Vol. 130). https://doi.org/10.1016/j.earscirev.2013.12.007

Bohren, C. F. (1983). *Absorption and scattering of light by small particles* (Vol. 35, p. 104). https://doi.org/10.1088/0031-9112/35/3/025

Bowie, A. R., Lannuzel, D., Remenyi, T. A., Wagener, T., Lam, P. J., Boyd, P. W., et al. (2009). Biogeochemical iron budgets of the Southern Ocean south of Australia: Decoupling of iron and nutrient cycles in the subantarctic zone by the summertime supply. *Global Biogeochemical Cycles*, *23*(4), GB4034. https://doi.org/10.1029/2009GB003500

Bowie, A. R., Maldonado, M. T., Frew, R. D., Croot, P. L., Achterberg, E. P., Mantoura, R. F. C., et al. (2001). The fate of added iron during a mesoscale fertilisation experiment in the Southern Ocean. *Deep-Sea Research Part II Topical Studies in Oceanography*, *48*(11–12), 11–12. https://doi.org/10.1016/S0967-0645(01)00015-7

Boyd, P. W. (2002). Environmental factors controlling phytoplankton processes in the. *Southern Ocean*, *38*(5), 844–861. https://doi.org/10.1046/j.1529-8817.2002.t01-1-01203.x

Boyd, P. W., Strzepek, R. F., Ellwood, M. J., Hutchins, D. A., Nodder, S. D., Twining, B. S., & Wilhelm, S. W. (2015). Why are biotic iron pools uniform across high- and low-iron pelagic ecosystems? *Global Biogeochemical Cycles*, *29*(7), 1028–1043. https://doi.org/10.1002/2014GB005014

Boye, M., van den Berg, C. M. G., de Jong, J. T. M., Leach, H., Croot, P., & De Baar, H. J. W. (2001). Organic complexation of iron in the Southern Ocean. *Deep Sea Research Part I: Oceanographic Research Papers*, *48*(6), 1477–1497. https://doi.org/10.1016/s0967-0637(00)00099-6

Browning, T. J., Bouman, H. A., & Moore, C. M. (2014). Satellite-detected fluorescence: Decoupling nonphotochemical quenching from iron stress signals in the South Atlantic and Southern Ocean. *Global Biogeochemical Cycles*, *28*(5), 510–524. https://doi.org/10.1002/2013GB004773

Brzezinski, M. A., Jones, J. L., & Demarest, M. S. (2005). Control of silica production by iron and silicic acid during the Southern Ocean Iron Experiment (SOFeX). *Limnology & Oceanography*, *50*(3), 810–824. https://doi.org/10.4319/lo.2005.50.3.0810

Coale, K. H., Johnson, K. S., Chavez, F. P., Buesseler, K. O., Barber, R. T., Brzezinski, M. A., et al. (2004). Southern Ocean iron enrichment experiment: Carbon cycling in high- and low-Si waters. *Science*, *304*(5669), 408–414. https://doi.org/10.1126/science.1089778

Croot, P. L., Bowie, A. R., Frew, R. D., Maldonado, M. T., Hall, J. A., Safi, K. A., et al. (2001). Retention of dissolved iron and FeII in an iron induced Southern Ocean phytoplankton bloom. *Geophysical Research Letters*, *28*(18), 3425–3428. https://doi.org/10.1029/2001GL013023

Duggen, S., Olgun, N., Croot, P., Hoffmann, L., Dietze, H., Delmelle, P., & Teschner, C. (2010). The role of airborne volcanic ash for the surface ocean biogeochemical iron-cycle: A review. *Biogeosciences*, *7*(3), 827–844. https://doi.org/10.5194/bg-7-827-2010

Dukes, D., Gonzales, H. B., Ravi, S., Grandstaff, D. E., Van Pelt, R. S., Li, J., et al. (2018). Quantifying postfire aeolian sediment transport using rare Earth element tracers. *Journal of Geophysical Research: Biogeosciences*, *123*(1), 288–299. https://doi.org/10.1002/2017JG004284

Falkowski, P. G., & LaRoche, J. (1991). *Acclimation To Spectral Irradiance in Algae*, (Vol. 27. pp. 8–14). https://doi.org/10.1111/j.0022-3646.1991.00008.x

Fan, G., Han, Z., Ma, W., Chen, S., Chai, F., Mazloff, M. R., et al. (2020). Southern Ocean carbon export efficiency in relation to temperature and primary productivity. *Scientific Reports*, *10*(1), 1–11. https://doi.org/10.1038/s41598-020-70417-z

Frenzel, H., Sharp, J., Fassbender, A., Buzby, N., Plant, J., Maurer, T., et al. (2021). BGC-Argo-Mat: A MATLAB toolbox for accessing and visualizing biogeochemical Argo data. *Zenodo*. https://doi.org/10.5281/zenodo.4971318

Frouin, R. J., Franz, B. A., Ibrahim, A., Knobelspiesse, K., Ahmad, Z., Cairns, B., et al. (2019). Atmospheric correction of satellite ocean-color imagery during the PACE era. *Frontiers of Earth Science*, *7*, 145. https://doi.org/10.3389/feart.2019.00145

Gabric, A. J., Cropp, R., McTainsh, G., Butler, H., Johnston, B. M., O'Loingsigh, T., & Van Tran, D. (2016). Tasman Sea biological response to dust storm events during the austral spring of 2009. *Marine and Freshwater Research*, *67*(8), 1090. https://doi.org/10.1071/MF14321

Gall, M. P., Boyd, P. W., Hall, J., Safi, K. A., & Chang, H. (2001). Phytoplankton processes. Part 1: Community structure during the Southern Ocean iron RElease experiment (SOIREE). *Deep-Sea Research Part II Topical Studies in Oceanography*, *48*(11–12), 11–12. https://doi.org/10.1016/S0967-0645(01)00008-X

Geider, R. J., MacIntyre, H. L., & Kana, T. M. (1996). A dynamic model of photoadaptation in phytoplankton. *Limnology & Oceanography*, *41*(1), 1–15. https://doi.org/10.4319/lo.1996.41.1.0001

Gelaro, R., McCarty, W., Suárez, M. J., Todling, R., Molod, A., Takacs, L., et al. (2017). The modern-era retrospective analysis for research and applications, version 2 (MERRA-2). *Journal of Climate*, *30*(14), 5419–5454. https://doi.org/10.1175/JCLI-D-16-0758.1

Halsey, K. H., & Jones, B. M. (2015). Phytoplankton strategies for photosynthetic energy allocation. *Annual Review of Marine Science*, *7*(1), 265–297. https://doi.org/10.1146/annurev-marine-010814-015813

Hamilton, D. S., Perron, M. M. G., Bond, T. C., Bowie, A. R., Buchholz, R. R., Guieu, C., et al. (2022). Earth, wind, fire, and pollution: Aerosol nutrient sources and impacts on ocean biogeochemistry. *Annual Review of Marine Science*, *14*(1), 303–330. https://doi.org/10.1146/annurev-marine-031921-013612

Hamilton, D. S., Scanza, R. A., Feng, Y., Guinness, J., Kok, J. F., Li, L., et al. (2019). Improved methodologies for Earth system modelling of atmospheric soluble iron and observation comparisons using the Mechanism of Intermediate complexity for Modelling Iron (MIMI v1.0). *Geoscientific Model Development*, *12*(9), 3835–3862. https://doi.org/10.5194/gmd-12-3835-2019

Hamme, R. C., Webley, P. W., Crawford, W. R., Whitney, F. A., Degrandpre, M. D., Emerson, S. R., et al. (2010). Volcanic ash fuels anomalous plankton bloom in subarctic northeast Pacific. *Geophysical Research Letters*, *37*(19), L19604. https://doi.org/10.1029/2010GL044629

Hayes, C. T., Fitzsimmons, J. N., Boyle, E. A., McGee, D., Anderson, R. F., Weisend, R., & Morton, P. L. (2015). Thorium isotopes tracing the iron cycle at the Hawaii Ocean Time-series Station ALOHA. *Geochimica et Cosmochimica Acta*, *169*, 1–16. https://doi.org/10.1016/j.gca.2015.07.019

Hiscock, M. R., Marra, J., Smith, W. O., Goericke, R., Measures, C., Vinke, S., et al. (2003). Primary productivity and its regulation in the Pacific sector of the Southern Ocean. *Deep-Sea Research Part II Topical Studies in Oceanography*, *50*(3–4), 533–558. https://doi.org/10.1016/S0967-0645(02)00583-0

Hoffmann, L. J., Peeken, I., Lochte, K., Assmy, P., & Veldhuis, M. (2006). Different reactions of Southern Ocean phytoplankton size classes to iron fertilization. *Limnology & Oceanography*, *51*(3), 1217–1229. https://doi.org/10.4319/lo.2006.51.3.1217

Hogle, S. L., Bundy, R. M., Blanton, J. M., Allen, E. E., & Barbeau, K. A. (2016). Copiotrophic marine bacteria are associated with strong iron-binding ligand production during phytoplankton blooms. *Limnology and Oceanography Letters*, *1*(1), 36–43. https://doi.org/10.1002/lol2.10026

Holte, J., Talley, L. D., Gilson, J., & Roemmich, D. (2017). An Argo mixed layer climatology and database. *Geophysical Research Letters*, *44*(11), 5618–5626. https://doi.org/10.1002/2017GL073426

Hutchins, D. A., DiTullio, G. R., & Burland, K. W. (1993). Iron and regenerated production: Evidence for biological iron recycling in two marine environments. *Limnology & Oceanography*, *38*(6), 1242–1255. https://doi.org/10.4319/lo.1993.38.6.1242

Ito, A., Myriokefalitakis, S., Kanakidou, M., Mahowald, N. M., Scanza, R. A., Hamilton, D. S., et al. (2019). Pyrogenic iron: The missing link to high iron solubility in aerosols. *Science Advances*, *5*(5), eaau7671. https://doi.org/10.1126/sciadv.aau7671

Ito, A., Ye, Y., Baldo, C., & Shi, Z. (2021). Ocean fertilization by pyrogenic aerosol iron. *npj Climate and Atmospheric Science*, *4*(1), 1–20. https://doi.org/10.1038/s41612-021-00185-8

Jickells, T. D., An, Z. S., Andersen, K. K., Baker, A. R., Bergametti, C., Brooks, N., et al. (2005). *Global iron connections between desert dust, ocean biogeochemistry, and climate*. https://doi.org/10.1126/science.1105959

Kablick, G. P., Allen, D. R., Fromm, M. D., & Nedoluha, G. E. (2020). Australian PyroCb smoke generates synoptic-scale stratospheric anticyclones. *Geophysical Research Letters*, *47*(13), e2020GL088101. https://doi.org/10.1029/2020GL088101

Kramer, S. J., Bisson, K. M., & Fischer, A. D. (2020). Observations of phytoplankton community composition in the Santa Barbara Channel during the Thomas Fire. *Journal of Geophysical Research: Oceans*, *125*(12), e2020JC016851. https://doi.org/10.1029/2020JC016851

Laglera, L. M., Tovar-Sánchez, A., Iversen, M. H., González, H. E., Naik, H., Mangesh, G., et al. (2017). Iron partitioning during LOHAFEX: Copepod grazing as a major driver for iron recycling in the Southern Ocean. *Marine Chemistry*, *196*, 148–161. https://doi.org/10.1016/j.marchem.2017.08.011

Liu, D., Zhou, C., Keesing, J. K., Serrano, O., Werner, A., Fang, Y., et al. (2022). Wildfires enhance phytoplankton production in tropical oceans. *Nature Communications*, *13*(1), 1348. https://doi.org/10.1038/s41467-022-29013-0

Mahowald, N. M., Baker, A. R., Bergametti, G., Brooks, N., Duce, R. A., Jickells, T. D., et al. (2005). *Atmospheric global dust cycle and iron inputs to the Ocean*, (Vol. 19). https://doi.org/10.1029/2004GB002402

Mallet, M. D., Desservettaz, M. J., Miljevic, B., Milic, A., Ristovski, Z. D., Alroe, J., et al. (2017). Biomass burning emissions in north Australia during the early dry season: An overview of the 2014 SAFIRED campaign. *Atmospheric Chemistry and Physics*, *17*(22), 13681–13697. https://doi.org/10.5194/acp-17-13681-2017

Martin, J. H., Gordon, R. M., & Fitzwater, S. E. (1990). Iron in Antarctic waters. *Nature*, *345*(6271), 156–158. https://doi.org/10.1038/345156a0

Mitchell, B. G., Brody, E. A., Holm-Hansen, O., McClain, C., & Bishop, J. (1991). Light limitation of phytoplankton biomass and macronutrient utilization in the Southern Ocean. *Limnology & Oceanography*, *36*(8), 1662–1677. https://doi.org/10.4319/lo.1991.36.8.1662

Mobley, C. D., Werdell, J., Franz, B., Ahmad, Z., & Bailey, S. (2016). *Atmospheric correction for satellite ocean color radiometryA tutorial and documentation NASA Ocean Biology processing group (June)*.

Morrison, A. K., Frölicher, T. L., & Sarmiento, J. L. (2015). Upwelling in the Southern Ocean. *Physics Today*, *68*(1), 27–32. https://doi.org/10.1063/pt.3.2654

Olgun, N., Duggen, S., Croot, P. L., Delmelle, P., Dietze, H., Schacht, U., et al. (2011). Surface ocean iron fertilization: The role of airborne volcanic ash from subduction zone and hot spot volcanoes and related iron fluxes into the Pacific Ocean. *Global Biogeochemical Cycles*, *25*(4), GB4001. https://doi.org/10.1029/2009GB003761

Orsi, A. H., Whitworth, T., & Nowlin, W. D. (1995). On the meridional extent and fronts of the Antarctic Circumpolar Current. *Deep-Sea Research Part I*, *42*(5), 641–673. https://doi.org/10.1016/0967-0637(95)00021-W

Perron, M. M. G., Meyerink, S., Corkill, M., Strzelec, M., Proemse, B. C., Gault-Ringold, M., et al. (2022). Trace elements and nutrients in wildfire plumes to the southeast of Australia. *Atmospheric Research*, *270*, 106084. https://doi.org/10.1016/j.atmosres.2022.106084

Perron, M. M. G., Proemse, B. C., Strzelec, M., Gault-Ringold, M., & Bowie, A. R. (2021). Atmospheric inputs of volcanic iron around Heard and McDonald Islands, Southern ocean. *Environmental Sciences: Atmosphere*, *1*(7), 508–517. https://doi.org/10.1039/D1EA00054C

Perron, M. M. G., Proemse, B. C., Strzelec, M., Gault-Ringold, M., Boyd, P. W., Rodriguez, E. S., et al. (2020). Origin, transport and deposition of aerosol iron to Australian coastal waters. *Atmospheric Environment*, *228*, 117432. https://doi.org/10.1016/j.atmosenv.2020.117432

Randles, C. A., da Silva, A. M., Buchard, V., Colarco, P. R., Darmenov, A., Govindaraju, R., et al. (2017). The MERRA-2 aerosol reanalysis, 1980 onward. Part I: System description and data assimilation evaluation. *Journal of Climate*, *30*(17), 6823–6850. https://doi.org/10.1175/JCLI-D-16-0609.1

Ryan-Keogh, T. J., Thomalla, S. J., Mtshali, T. N., Van Horsten, N. R., & Little, H. J. (2018). Seasonal development of iron limitation in the sub-Antarctic zone. *Biogeosciences*, *15*(14), 4647–4660. https://doi.org/10.5194/bg-15-4647-2018

Sakshaug, E., Slagstad, D., & Holm-Hansen, O. (1991). Factors controlling the development of phytoplankton blooms in the Antarctic Ocean — a mathematical model. *Marine Chemistry*, *35*(1–4), 259–271. https://doi.org/10.1016/S0304-4203(09)90021-4

Sato, M., Takeda, S., & Furuya, K. (2007). Iron regeneration and organic iron(III)-binding ligand production during in situ zooplankton grazing experiment. *Marine Chemistry*, *106*(3–4), 471–488. https://doi.org/10.1016/j.marchem.2007.05.001

Schallenberg, C., Bestley, S., Klocker, A., Trull, T. W., Davies, D. M., Gault-Ringold, M., et al. (2018). Sustained upwelling of subsurface iron supplies seasonally persistent phytoplankton blooms around the southern Kerguelen Plateau, Southern Ocean. *Journal of Geophysical Research: Oceans*, *123*(8), 5986–6003. https://doi.org/10.1029/2018JC013932

Schollaert, S. E., Yoder, J. A., O'Reilly, J. E., & Westphal, D. L. (2003). Influence of dust and sulfate aerosols on ocean color spectra and chlorophyll a concentrations derived from SeaWiFS off the U.S. East Coast. *Journal of Geophysical Research*, *108*(6), 3191. https://doi.org/10.1029/2000jc000555

Sedwick, P. N., Blain, S., Quéguiner, B., Griffiths, F. B., Fiala, M., Bucciarelli, E., & Denis, M. (2002). Resource limitation of phytoplankton growth in the Crozet basin, subantarctic Southern Ocean. *Deep-Sea Research Part II Topical Studies in Oceanography*, *49*(16), 3327–3349. https://doi.org/10.1016/S0967-0645(02)00086-3

Shi, Z., Krom, M. D., Bonneville, S., Baker, A. R., Bristow, C., Drake, N., et al. (2011). Influence of chemical weathering and aging of iron oxides on the potential iron solubility of Saharan dust during simulated atmospheric processing. *Global Biogeochemical Cycles*, *25*(2), GB2010. https://doi.org/10.1029/2010GB003837

Sunda, W. G., & Huntsman, S. A. (1995). Iron uptake and growth limitation in oceanic and coastal phytoplankton. *Marine Chemistry*, *50*(1–4), 189–206. https://doi.org/10.1016/0304-4203(95)00035-P

Tagliabue, A., Bopp, L., & Aumont, O. (2009). Evaluating the importance of atmospheric and sedimentary iron sources to Southern Ocean biogeochemistry. *Geophysical Research Letters*, *36*(13), L13601. https://doi.org/10.1029/2009GL038914

Tagliabue, A., Sallée, J. B., Bowie, A. R., Lévy, M., Swart, S., & Boyd, P. W. (2014). Surface-water iron supplies in the Southern Ocean sustained by deep winter mixing. *Nature Geoscience*, *7*(4), 314–320. https://doi.org/10.1038/ngeo2101

Tang, W., Llort, J., Weis, J., Perron, M. M. G., Basart, S., Li, Z., et al. (2021). Widespread phytoplankton blooms triggered by 2019–2020 Australian wildfires. *Nature*, *597*(7876), 370–375. https://doi.org/10.1038/s41586-021-03805-8

Thuróczy, C. E., Gerringa, L. J., Klunder, M. B., Laan, P., & de Baar, H. J. (2011). Observation of consistent trends in the organic complexation of dissolved iron in the Atlantic sector of the Southern Ocean. *Deep-Sea Research Part II Topical Studies in Oceanography*, *58*(25–26), 2695–2706. https://doi.org/10.1016/j.dsr2.2011.01.002

Twelves, A. G., Goldberg, D. N., Henley, S. F., Mazloff, M. R., & Jones, D. C. (2021). Self-shading and meltwater spreading control the transition from light to iron limitation in an Antarctic coastal polynya. *Journal of Geophysical Research: Oceans*, *126*(2), e2020JC016636. https://doi.org/10.1029/2020JC016636

Twining, B. S., Baines, S. B., Fisher, N. S., & Landry, M. R. (2004). Cellular iron contents of plankton during the Southern Ocean iron experiment (SOFeX). *Deep-Sea Research Part I Oceanographic Research Papers*, *51*(12), 1827–1850. https://doi.org/10.1016/j.dsr.2004.08.007

Vaillancourt, R. D., Brown, C. W., Guillard, R. R. L., & Balch, W. M. (2004). Light backscattering properties of marine phytoplankton: Relationships to cell size, chemical composition and taxonomy. *Journal of Plankton Research*, *26*(2), 191–212. https://doi.org/10.1093/plankt/fbh012

Wagner, R., Jähn, M., & Schepanski, K. (2018). Wildfires as a source of airborne mineral dust - revisiting a conceptual model using large-eddy simulation (LES). *Atmospheric Chemistry and Physics*, *18*(16), 11863–11884. https://doi.org/10.5194/acp-18-11863-2018

Wang, W., Luo, C., Sheng, L., Zhao, C., Zhou, Y., & Chen, Y. (2021). Effects of biomass burning on chlorophyll-a concentration and particulate organic carbon in the subarctic north Pacific ocean based on satellite observations and WRF-chem model simulations: A case study. *Atmospheric Research*, *254*, 105526. https://doi.org/10.1016/j.atmosres.2021.105526

Wang, Y., Chen, H. H., Tang, R., He, D., Lee, Z., Xue, H., et al. (2022). Australian fire nourishes ocean phytoplankton bloom. *The Science of the Total Environment*, *807*, 150775. https://doi.org/10.1016/j.scitotenv.2021.150775

Westberry, T. K., Behrenfeld, M. J., Milligan, A. J., & Doney, S. C. (2013). Retrospective satellite ocean color analysis of purposeful and natural ocean iron fertilization. *Deep-Sea Research Part I Oceanographic Research Papers*, *73*, 1–16. https://doi.org/10.1016/j.dsr.2012.11.010

Westberry, T. K., Shi, Y. R., Yu, H., Behrenfeld, M. J., & Remer, L. A. (2019). Satellite-detected ocean ecosystem response to volcanic eruptions in the subarctic northeast Pacific Ocean. *Geophysical Research Letters*, *46*(20), 11270–11280. https://doi.org/10.1029/2019GL083977

Whicker, J. J., Pinder, J. E., & Breshears, D. D. (2006). Increased wind erosion from forest wildfire: Implications for contaminant-related risks. *Journal of Environmental Quality*, *35*(2), 468–478. https://doi.org/10.2134/jeq2005.0112

Whitmire, A. L., Pegau, W. S., Karp-Boss, L., Boss, E., & Cowles, T. J. (2010). Spectral backscattering properties of marine phytoplankton cultures. *Optics Express*, *18*(14), 15073. https://doi.org/10.1364/oe.18.015073

Winton, V. H. L., Edwards, R., Bowie, A. R., Keywood, M., Williams, A. G., Chambers, S. D., et al. (2016). Dry season aerosol iron solubility in tropical northern Australia. *Atmospheric Chemistry and Physics*, *16*(19), 12829–12848. https://doi.org/10.5194/acp-16-12829-2016

Wolff, G. A., Billett, D. S. M., Bett, B. J., Holtvoeth, J., FitzGeorge-Balfour, T., Fisher, E. H., et al. (2011). The effects of natural iron fertilisation on deep-sea ecology: The Crozet Plateau, southern Indian Ocean. *PLoS One*, *6*(6), e20697. https://doi.org/10.1371/journal.pone.0020697

Zheng, L., & Sohrin, Y. (2019). Major lithogenic contributions to the distribution and budget of iron in the North Pacific Ocean. *Scientific Reports*, *9*(1), 11652. https://doi.org/10.1038/s41598-019-48035-1